Evaluation of temperature effect on inductance computation in variable magnetic components for Dual-Active-Bridge application

Sarah Saeed[1], Jorge Garcia[1], Marina S. Perdigão[2,3], Valter S. Costa[2,4], and Ramy Georgious[1,5]
[1] *University of Oviedo*, Department of Electrical Engineering, Spain,
[2] *Instituto de Telecomunicações*, Coimbra, Portugal,
[3] *Coimbra Polytechnic - ISEC*, Coimbra, Portugal,
[4] *University of Coimbra*, Department of Electrical and Computer Engineering, Portugal,
[5] *Port Said University*, Department of Electrical Engineering, Egypt.
email: saeedsarah@uniovi.es

***Abstract*— This work presents a thorough study of the impact of the operating temperature of the magnetic core on the computed value of the inductance in a power electronic converter at different operation conditions. The analysis is specifically interesting in the case of variable magnetic components. In general, the core temperature varies as a function of several parameters, such as the ambient temperature, the excitation current applied to the inductor windings –which causes core and winding losses and results in heating of the magnetic material– and finally the thermal conductivity of the magnetic material. To decouple the different factors affecting the inductance, Finite Element Analysis simulations are carried out for a variable inductor as a case study. Reinforced by this analysis, a final lookup table/map is proposed to accurately scale the inductance variation range predicted by the analytical design methods in order to match the practical measurements under different excitation currents.**

Keywords—temperature effect, variable magnetics, design, FEA.

I. INTRODUCTION

The careful design of power inductors for power electronic converters plays an essential role in the performance of the whole system, as it can significantly impact key aspects such as the complexity, the efficiency, the size, and the power density of the converter. Therefore, it is necessary to develop accurate device models and also to study design limitations, such as material saturation, core losses, thermal design, etc.

The magnetic device of interest is the variable inductor (VI). It presents a highly desirable case study since the model developed for the VI can be directly extended to analyze other nonlinear and multi-winding magnetic devices [1]. Moreover, in recent literature, there has been a growing direction to employ the VI in a wide range of applications [2]-[7]. The VI allows for additional degrees of freedom in the design and control of power electronic converters. This is distinctly useful in resonant converters, where the usual frequency control has some drawbacks due to Electro-Magnetic Interference (EMI) issues, synchronization, variable sampling time, etc., especially for large ranges of variation. If variable magnetics are used, the same control margins can be obtained at a constant switching frequency, therefore allowing for an optimization of the EMI filters, and sampling procedures. In other applications such as the Dual Active Bridge (DAB) converter, in addition to adding a new degree of freedom to the control, the inclusion of variable magnetics can increase operation parameters such as the soft switching margins, etc. [1][8][9].

One of the issues of modeling the VI is the inaccuracy of the estimation of the amount of inductance variation within the control range of the device. This issue arises due to the ill-defined material properties under saturation conditions [10]. In some previous works [10][11], accurate definitions for the magnetic material properties, such as the permeability, the B(H) curve, and the distribution of saturated regions in the core, have been defined and well-validated specifically under saturation of the VI magnetic core. However, specific to the issue of estimation of the inductance variation range, the effect of the core temperature has not been considered during modeling the VI. The variation of the core temperature under different operation conditions of the device would alter the characteristic B(H) of the ferrite material, causing a considerable shift of the inductance value especially at high saturation levels [11].

It is nontrivial to predict the magnetic core temperature since it is affected by several factors [12]. On one side, the core and winding losses resulting from the current applied to the windings of the device are the main sources of heating of the core. Also, on another side, the ambient temperature affects the core temperature based on the thermal conductivity of the material. And finally, a combination of radiation and convection thermal processes dissipates this heat from the exposed surfaces of the magnetic core. The temperature rise of the core is thus difficult to predict with precision [12]. This work presents a thorough analysis to decouple the different factors affecting the core temperature and proposes a corresponding correction factor which scales the inductance variation range to match the practical measured values under different excitation currents.

In this context, section II presents the different approaches for computing the inductance in variable magnetics. Later in section III, the temperature effect on the inductance value is analyzed by carrying out experimental tests, as well as Finite Element Analysis (FEA). Section IV explains the proposed correction factor for the inductance variation range, in addition to the experimental validation of the proposed calculation procedure. And finally, section V summarizes the conclusions of the work and future perspectives.

The present work has been partially supported by the European Union's H2020 Research and Innovation programme under Grant Agreement No. 864459 (UE-19-TALENT-864459). Also, the work has been partially supported by the Spanish Government (Innovation Development and Research Office-MEC) under the research grant ENE2016-77919, "Conciliator" Project, and also "B2B" Project Nuevas vías hacia la gestión descentralizada de la energía de edificio a edificio PID2019-111051RB-100. The work has been partially supported also by the government of the Principality of Asturias, grant no. FC-GRUPIN-IDI/2018/000241, and under "Severo Ochoa" program of predoctoral grants for training in research and university teaching, grant number BP16-133. The work has been partially supported also by Instituto de Telecomunicações, Coimbra, Portugal, with financial support reference: UID/EEA/50008/2019.

II. Inductance Computation in Variable Inductor

Specific to this study, the VI structure used is the double E-core assembly [13] depicted in Fig. 1a. Due to the main winding (N_{ac}), an AC flux (ϕ_C) circulates through the center arm and splits to the outer arms. Applying a relatively small DC current (I_b) to the bias control windings (N_b), a DC flux (ϕ_R or ϕ_L) is produced which circulates mainly through the outer (ungapped) circumference of the core [13]. This flux can bias the operation point of the magnetic material towards the nonlinear region, causing the inductance seen from the main winding terminals to vary [14][15].

The operation is clarified by Fig. 1b, which shows the operation points on the B(H) curve for the left and right arms. The constant DC control current will produce a constant magnetomotive force (*mmf)* in the left and right arms, N_bI_b, which will bring these sections into the non-linear region of the magnetization curve.

The inductance can be defined in different ways with respect to the B(H) curve. The first definition, which is also considered as the general definition, states that the inductance, L, is the ratio of the total flux linkage to the current flowing through the winding [13], as expressed by (1).

$$L = \frac{N_{ac}\Phi_C}{i_{ac}}, \tag{1}$$

where N_{ac} is the number of turns of the main winding, ϕ_C is the AC flux linking this winding, and i_{ac} is the AC current flowing through the winding. This definition is satisfactory for a medium with a constant permeability, such as air. However, for ferromagnetic materials, a differential inductance is defined, dL, as expressed by (2).

$$dL = \frac{N_{ac}d\Phi_C}{di_{ac}} \tag{2}$$

And finally, considering the reluctance model [14][15], the inductance can be calculated based on the reluctances of different paths in the magnetic circuit, as defined by Fig. 2, in order to obtain the inductance as a function of the DC bias control current [16][17].

Fig. 2a illustrates the lengths of different reluctance paths and Fig. 2b shows the equivalent reluctance circuit model of this magnetic core. The reluctance of a magnetic path is defined by (3).

$$\mathcal{R}_i = \frac{l_i}{\mu_i . A_i}, \tag{3}$$

where l_i is the length of the path i, μ_i is the permeability of the magnetic material, and A_i is the cross sectional area. The inductance can thus be calculated based on the reluctance of different paths in the magnetic circuit, as shown by (4).

$$L = \frac{{N_{ac}}^2}{\mathcal{R}_7+\mathcal{R}_{gap}+\mathcal{R}_8+(\mathcal{R}_1+\mathcal{R}_3+\mathcal{R}_{gl}+\mathcal{R}_4+\mathcal{R}_9)//(\mathcal{R}_2+\mathcal{R}_5+\mathcal{R}_{gl}+\mathcal{R}_6+\mathcal{R}_{10})} \tag{4}$$

Assuming symmetry of the geometrical core dimensions and operation, the inductance expression reduces to (5).

$$L = \frac{{N_{ac}}^2}{\mathcal{R}_{gap}+2\mathcal{R}_7+\mathcal{R}_1+\mathcal{R}_3} \tag{5}$$

The inductance value calculated by (5) represents the maximum inductance of the variable inductor, i.e. with no DC bias current applied to the control windings, while the minimum inductance value depends on the saturation level of the magnetic core. The saturated magnetic paths present a different reluctance value, $\mathcal{R}_{isat}$, which is a function of the saturated path length, l_{isat}, and the differential permeability value corresponding to the level of saturation [11], as explained by (6).

$$\mathcal{R}_{isat} = \frac{l_{isat}}{\mu_{isat}A_i} \tag{6}$$

Only the outer frame of the core is saturated, therefore the reluctances associated with these paths are modified under saturation [11], as clarified by Fig. 3. Consequently, the minimum inductance provided by the variable inductor can be calculated by recalculating the reluctances of the saturated magnetic paths and substituting the values in (5). The resulting expression for the minimum inductance is stated by (7).

$$L_{min} = \frac{{N_{ac}}^2}{\mathcal{R}_{gap}+2\mathcal{R}_7+\mathcal{R}_{1sat}+\mathcal{R}_{3sat}} \tag{7}$$

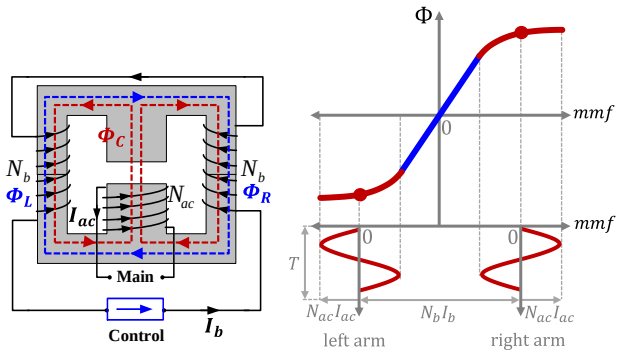

Fig. 1. Variable inductor based on double E-core [13]. a) Structure and windings, and b) principle of operation.

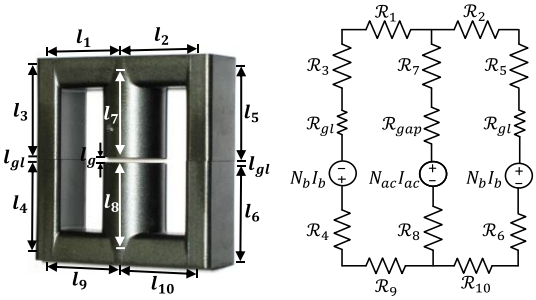

Fig. 2. Reluctance circuit. a) Lengths of reluctance paths, and b) the corresponding circuit model.

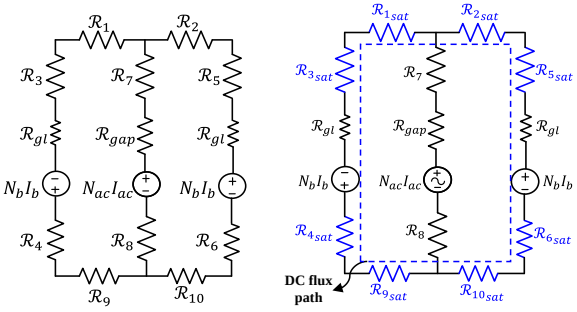

Fig.3. Reluctance circuit model, a) under no saturation, and b) under saturation.

III. Inductance Shift over Temperature

In ferrite core variable inductors, increasing the power level of operation, i.e. increasing AC *mmf*, will result in a rise in the temperature of the magnetic core. This temperature rise affects the B(H) curve of the magnetic core; with the increase of temperature, maximum magnetic flux density decreases. This will result in a reduced permeability and, consequently, a higher reluctance value which will result in a lower inductance value. However, besides the temperature effect, the AC *mmf* level in itself affects the inductance value, especially under a nonlinear operation of the core. This takes place because the change in AC *mmf* will result in a change in the AC flux in the main arm of the core, which directly affects the value of the inductance measured from the winding across this arm (main winding).

To this extent, the following sections present experimental results to show the effect of the core temperature on the inductance value. And in order to decouple the effects of core temperature and AC *mmf*, FEA simulations are carried out.

A. Experimental measurements of core temperature

As it was mentioned previously, the core temperature, T_c, is affected by several factors, basically summarized to:

- Ambient temperature, T_a, which impacts the core temperature based on the material thermal conductivity.
- Excitation current applied to the inductor windings, which in the case of the VI are the AC current, i_{ac}, applied to the main winding, and the DC bias current, I_b, applied to the control windings.
- The dissipation of heat from the exposed magnetic surface as a combination of radiation and convection [18].

Some experiments are thus carried out to measure the core temperature, and relate it to the AC and DC currents in the VI windings. Moreover, the tests are repeated for different ambient temperatures to include the effect of the surroundings temperature on the core.

Fig. 4 shows a circuit diagram of the developed test platform. It consists of a SiC DAB converter in which the conventional constant inductor has been replaced by a variable one [1], with the specifications in Table I. The converter is controlled by using the TMS320F28335 peripheral board. Additionally, a variable DC voltage supply is connected in series with a resistor to provide a DC control current of maximum 1.2A to the control windings of the VI. The constructed test platform is illustrated in Fig. 5.

Two tests have been carried out at two different input voltage levels, V_{in}, 50V, and 100V. At each operation condition, the inductance value is varied from maximum to minimum values by means of varying the control current from 0 to 1.2A. The inductance value is calculated using the RMS values of the first harmonic component of the voltage and current measurements, so the resulting inductance is computed by (8).

$$L = \frac{X_L}{\omega} = \frac{V_L}{I_{ac}} \cdot \frac{\pi/4}{2\pi \cdot f}, \qquad (8)$$

where V_L is the RMS value of the voltage measured across the main winding of the VI, I_{ac} is the RMS value of AC current flowing through this winding, and f is the switching frequency, which is 50kHz for the tests carried out.

The measured inductance curves are illustrated in Fig. 6a as a function of the control current for each of the tested voltage levels. It can be observed that as the voltage level of operation is increased, which also indicates an increase in the AC *mmf* applied to the inductor main winding, the inductance variation range decreases.

As explained before, the change in the AC *mmf* directly affects the inductance value since it causes a change in the AC flux generated in the main arm. However, the increase in the AC *mmf* results in core and winding losses. These losses boost the core temperature modifying the properties of the magnetic material. To test this effect, the first approach taken is performing experimental measurements to record the variation of the core temperature corresponding to the latter two tests.

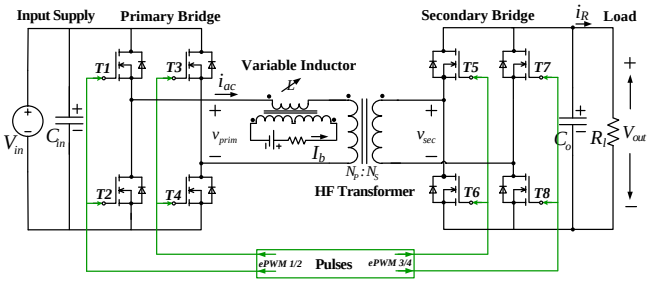

Fig. 4. Circuit diagram of test platform.

TABLE I. Specifications of VI Prototype

Core size	ETD49/25/16
Magnetic material	Ferrite N87
Inductance variation range	144 µH to 51 µH
No. turns of main winding, N_{ac}	23
No. turns of each control winding, N_b	55
Airgap length, l_g	1 mm

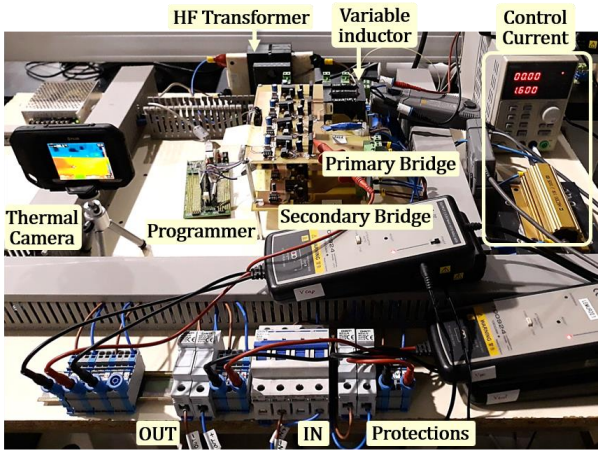

Fig. 5. Experimental setup used to test the variable inductor under large-signal analysis.

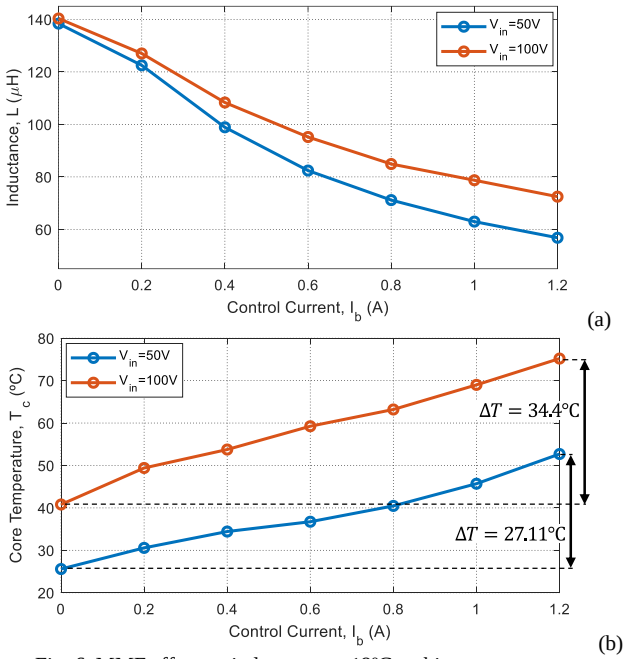

Fig. 6. MMF effect on inductance at 18ºC ambient temperature. a) Measured inductance, and b) corresponding measured core temperature as a function of bias current.

The core temperature, T_c, is measured by *NTC* thermistors. The readings of the *NTC* are recorded using a *PicoLog TC-08* which is a thermocouple data logger device from *Pico Technology*® [19]. The device provides an extra advantage over the analytical calculation of the temperature, which is the ability to follow the trend of temperature variation through a real-time data acquisition software, as illustrated by Fig. 7. This allows to make sure that the core temperature has reached steady-state to record an accurate value. By observation, for each 0.1A step in bias current, the core is left around 20 minutes to settle down before taking the temperature measurement, moreover, the core is left around 1.5 hours to settle down to the initial temperature between each of the two tests.

The temperature curves as a function of the control current were recorded during each of the two tests, $50V_{in}$ and $100V_{in}$, as seen in Fig. 6b. As observed from the plot, the measured temperature rise of the magnetic core at the maximum DC bias current of 1.2A is recorded to be 27.11ºC for the test at $50V_{in}$, and 34.4ºC for the test at $100V_{in}$.

It can be concluded that the inductance curves shift up as the voltage level is increased. The values show larger dispersion as the control current is increased. This augmentation of the inductance is attributed to the AC *mmf* as well as the core temperature rise as explained earlier.

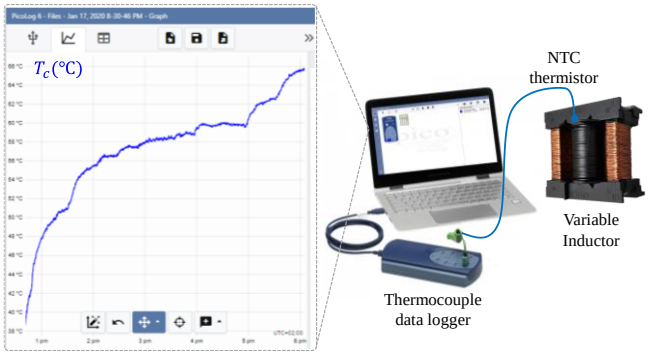

Fig. 7. Real-time magnetic core temperature measurement by using NTC sensor, and a thermocouple device to scale the measurements to temperature readings.

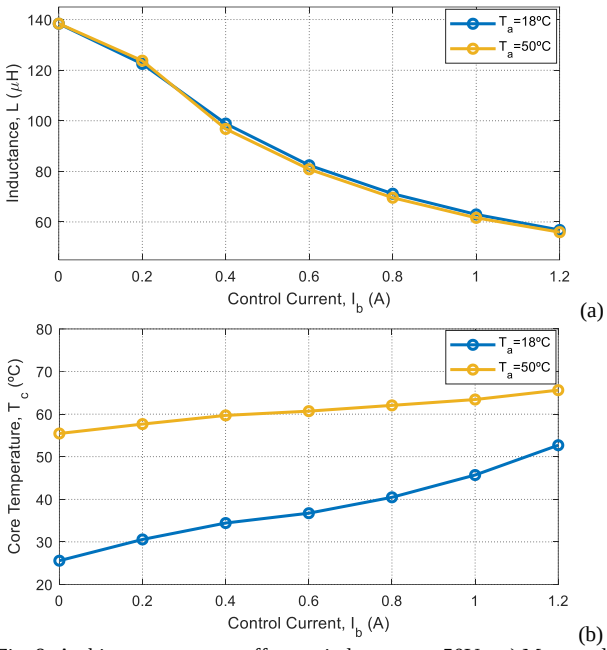

Fig. 8. Ambient temperature effect on inductance at $50V_{in}$. a) Measured inductance, and b) corresponding measured core temperature, as a function of bias current.

It is worth to note that the temperature rise of the magnetic core can be estimated analytically. This can be done by using the empirical formulas provided by some core manufacturers which computes the temperature rise of the core as a function of the total losses of the device [20][21].

On the other hand, the effect of the ambient temperature on the inductance is also studied. For this, the test at 50V was repeated at different ambient temperatures, T_a, of 18ºC and 50ºC. The ambient temperature was varied by means of closing the surroundings of the VI using a metal box, and applying a heater fan on the outer frame of the box.

Fig. 8a illustrates the measured inductance during the latter test, while Fig. 8b shows the corresponding core temperature. It is observed that under a 30ºC increase in the ambient temperature, the inductance curve is slightly shifted down, around 3µH decrease. While, at the points of 0A and 1.2A bias, almost no variation in the inductance takes place. This shows that the ambient temperature has a relatively small effect on the inductance value. However, it would be interesting to extend this conclusion to a wider range of temperature variation. This can be done by using a thermal chamber to provide lower as well as higher ambient temperatures.

B. Finite element analysis simulations

The software package used for FEA simulations is *Altair Flux*™ [22]. An FEA model has been developed and validated as part of a previous work [11]. Briefly, the FEA simulation is developed in three main steps: first, the construction of the 3D core geometry and the mesh generation. Second, adjusting the physical properties which include defining the materials of the magnetic core and the coils, constructing coil conductors, and assigning different volumes regions. And thirdly, solving the constructed magnetic device under certain scenarios of parameters.

Fig. 9 illustrates the 3D constructed model for the VI, as well as the developed prototype.

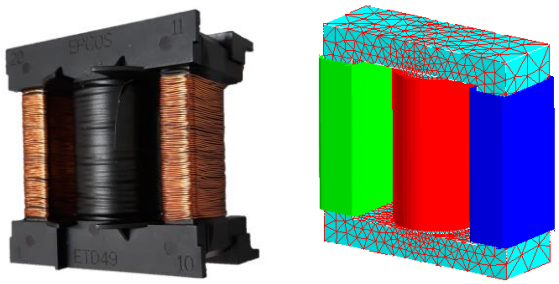

(a) (b)

Fig. 9. Variable inductor. a) Prototype based on double E-core, and b) constructed 3D model in *Flux*™.

As it has been clarified previously, there is a cross-coupling between the core temperature and the AC *mmf* effects on the value of the inductance. Therefore, there is no direct relationship that can describe the inductance variation as a function of the core temperature nor the AC *mmf* separately.

The solution is to decouple the effects of both factors, and to generate some kind of 3D lookup table/map to explain the inductance as function of, not only the DC control current, but also the AC *mmf*, and reproduce this map for different core temperatures. To this motivation, FEA simulations were carried out to study the effect of each factor alone.

During the first simulation, the AC *mmf* is kept constant while the core temperature is increased from 25ºC to 100ºC, by configuring the corresponding B(H) curve of the magnetic material at these temperature values. The inductance is thus computed as a function of the bias control current, Fig. 10a. It can be observed from the plot that the inductance curves shift down as the core temperature is increased.

During the second simulation, the core temperature is kept constant at 25ºC, while the AC *mmf* is changed, by varying I_{ac}. Fig. 10b shows the inductance curves as a function of the bias control current. It can be observed that the inductance value increases as I_{ac} is increased from 1A to 6A.

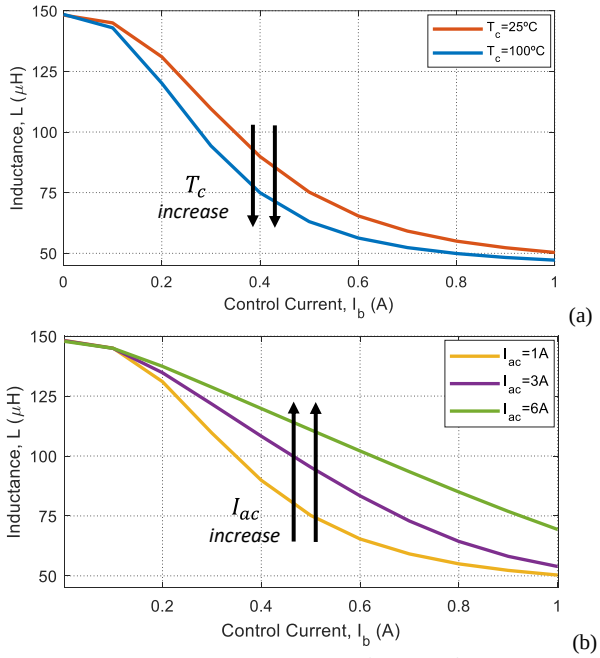

Fig. 10. FEA simulations. Inductance as a function of the bias control current, at: a) different core temperatures, and b) different AC RMS currents.

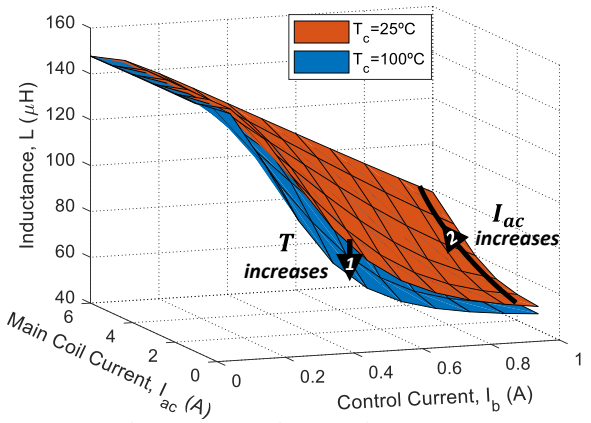

Fig. 11. 3D map of inductance as a function of control current, I_b, and main current, I_{ac}, for different values of core temperature, T_c.

Combining the curves in Fig. 10, the inductance value can be represented as a function of the control current as well as the main winding RMS current for different temperature values, 25ºC and 100ºC, as it is illustrated in Fig. 11.

Two observations can be made from this figure; first, it can be seen that going from 25ºC to 100ºC temperature, the values of $L(I_b,I_{ac})$ is decreased almost in a linear manner (curve translated downwards as clarified by arrow 1), and second, as I_b increases from 0 to 1 A the effect of I_{ac} on the inductance becomes more significant as it is clarified by arrow 2. The arrow shows that the minimum inductance value, i.e. the inductance value at the maximum DC bias current I_b =1A, increases as a function of I_{ac}. This change in the inductance value can be accounted for at the design stage of the variable inductor, as it will be explained in the following section.

IV. Correction of Inductance Variation Range

Based on the previous analysis, an inevitable shift in the inductance value will take place at different operation conditions of the VI. Therefore, a readjustment of the design of the VI is necessary.

Consequently, in this section, a correction factor is formulated to scale the inductance variation range computed by the theoretical design rules in order to take into account the practical operation conditions, which are mainly reduced to two factors the AC current and the core temperature, as analyzed in the previous sections.

A. Correction factor

Due to any change in the magnetic core temperature or the AC *mmf*, the L_{min} predicted by the design of the VI will be different from the experimental value. Using the FEA analysis carried out previously, the L_{min} estimated by the theoretical design can be corrected on a basis of multiplying L_{max} by a correction factor. This factor is a function of the temperature as well as the AC *mmf*.

For this reason, it is essential to define the inductance range ratio, r_a [16]. It is the ratio between the maximum and the minimum inductance, as explained by (9).

$$r_a = \frac{L_{max}}{L_{min}} \tag{9}$$

Accordingly, L_{min} is calculated by multiplying L_{max} by the factor $1/r_a$. Therefore, if r_a could be computed as a function of the temperature and the AC *mmf*, the corrected L_{min} could be obtained.

To generalize the study for any required design values, a normalized factor, f_{corr} is obtained, which is defined by (10).

$$f_{corr} = \frac{r_a}{r_a^*}, \tag{10}$$

where r_a^* is the theoretical design range ratio, calculated at 25ºC and I_{ac}=1A.

Fig. 12 illustrates the curves for f_{corr} as a function of I_{ac} for two different core temperature values. As it can be observed the value of the correction factor is 1 at the design point at 25ºC, and decreases below 1 for different values of I_{ac}.

Correspondingly, the corrected L_{min} is calculated by (11).

$$L_{min} = L_{max} \cdot \frac{1}{r_a^* \cdot f_{corr}} \tag{11}$$

B. *Experimental validation*

For the specific VI design constructed herein, whose specifications are stated previously in Table I, the maximum and minimum inductance values are calculated as previously explained by (5) and (7), respectively. This is done by substituting the reluctance lengths and permeability values corresponding to each magnetic path at no saturation for calculating the L_{max}, and at the full saturation for calculating L_{min}. The computation of those inductance values is clarified by (12) and (13).

$$L_{max} = \frac{{N_{ac}}^2}{\frac{l_g}{\mu_0 A_c} + 2\frac{l_7}{\mu_0 \mu_d A_c} + \frac{l_1}{\mu_0 \mu_d A_b} + \frac{l_3}{\mu_0 \mu_d A_b}}$$
$$= \frac{23^2}{\frac{1e^{-3}}{4\pi*10^{-7}*207.39e^{-6}} + 2\frac{20.95e^{-3}}{8.4e^{-3}*207.39e^{-6}} + \frac{21.5e^{-3}}{8.4e^{-3}*105.56e^{-6}} + \frac{21.44e^{-3}}{8.4e^{-3}*105.56e^{-6}}}$$
$$= 144\mu H \tag{12}$$

$$L_{min} = \frac{{N_{ac}}^2}{\frac{l_g}{\mu_0 A_c} + 2\frac{l_7}{\mu_0 \mu_d A_c} + \frac{l_{1sat}}{\mu_0 \mu_{dsat} A_b} + \frac{l_{3sat}}{\mu_0 \mu_{dsat} A_b}}$$
$$= \frac{23^2}{\frac{1e^{-3}}{4\pi*10^{-7}*207.39e^{-6}} + 2\frac{20.95e^{-3}}{8.4e^{-3}*207.39e^{-6}} + \frac{15.8e^{-3}}{5e^{-5}*105.56e^{-6}} + \frac{19.8e^{-3}}{5e^{-5}*105.56e^{-6}}}$$
$$= 51\mu H \tag{13}$$

Therefore, the inductance range ratio calculated through the design process is stated by (14) [11][16].

$$r_a^* = \frac{L_{max}}{L_{min}} \approx 2.8 \tag{14}$$

Using the correction factor obtained from the FEA simulations, the corrected L_{min} that the VI can provide in practice is calculated at the expected operating conditions of AC *mmf* and temperature.

To be able to validate the proposed correction factor, the experiments carried out, and illustrated in Fig. 6, are repeated for five different operation points by varying the input voltage V_{in}= 10, 30, 50, 70, 100V. The corresponding L_{min} is calculated at the maximum bias current of 1.2A, by measuring the AC inductor voltage and current, as previously explained by (8).

Based on the values of I_{ac} and T_c, the corresponding correction factor is also extracted from Fig. 12. Using linear interpolation, f_{corr} can be obtained at any current or temperature values. Therefore, the corrected minimum inductance can be computed for each of the operation points, as clarified by Table II.

To have a visual comparison, the corrected L_{min} values, stated in Table II, are illustrated by Fig. 13 in comparison with the experimental values of the minimum inductance to prove the validity under the full range of operation in which I_{ac} varies between 1A and 6A. Also, the design value, calculated by (13) to be 51µH, is included in the figure for comparison.

It can be observed that the corrected inductance matches the experimental measurement with increased accuracy compared to the design value, especially at higher I_{ac} values.

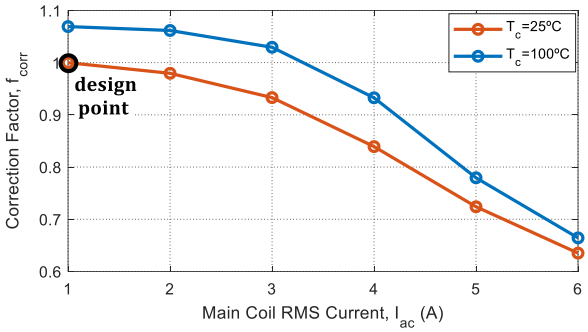

Fig. 12. Correction factor for the design of the variable inductor.

TABLE II. CALCULATION OF CORRECTED MINIMUM INDUCTANCE

V_{in}	I_{ac}	T_c	f_{corr}	Corrected L_{min}
10V	0.8A	30ºC	0.99	$\frac{L_{max}}{r_a^* \cdot f_{corr}} = \frac{144}{2.8*0.99} = 51.4\mu H$
30V	2.3A	40ºC	0.93	$\frac{L_{max}}{r_a^* \cdot f_{corr}} = \frac{144}{2.8*0.93} = 55.1\mu H$
50V	3.8A	50ºC	0.85	$\frac{L_{max}}{r_a^* \cdot f_{corr}} = \frac{144}{2.8*0.85} = 60.5\mu H$
70V	4.4A	60ºC	0.79	$\frac{L_{max}}{r_a^* \cdot f_{corr}} = \frac{144}{2.8*0.79} = 65.1\mu H$
100V	5.45A	75ºC	0.7	$\frac{L_{max}}{r_a^* \cdot f_{corr}} = \frac{144}{2.8*0.7} = 73.5\mu H$

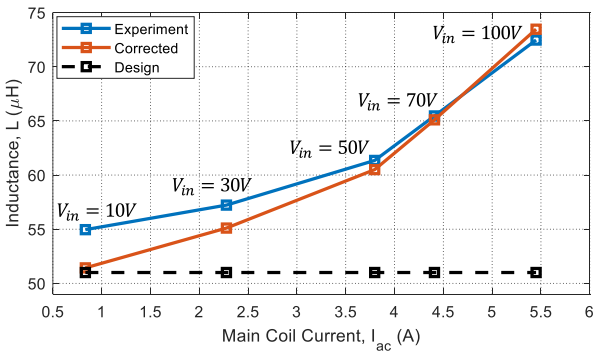

Fig. 13. Corrected inductance value at 1.2A DC bias current compared to experimental measurements.

V. Conclusions

The work presented an evaluation of the core temperature effect on the inductance variation range in variable magnetic elements. Different factors affecting the core temperature have been decoupled using FEA simulations.

A DAB converter prototype is developed to validate the predicted inductance shift of the variable inductor under different AC and DC excitation currents. Through accurate real-time experimental measurements, the temperature of the magnetic core is recorded, and applying the proposed correction factor, the corrected inductance is observed to match the measured one with extended accuracy compared to the analytical design procedure. The study leads to an improvement in the design of the variable inductor to predict more accurate inductance variation range specifically under high saturation.

For future work, an empirical expression can be used to estimate the core temperature rise as a function of the core and winding losses of the variable inductor. Also, the study of the ambient temperature effect could be extended by increasing the range of temperature variation. This can be carried out by means of a thermal chamber to acquire lower as well as higher degrees.

References

[1] S. Saeed and J. Garcia, "Extended Operational Range of Dual-Active-Bridge Converters by using Variable Magnetic Devices," 2019 IEEE Applied Power Electronics Conference and Exposition (APEC), Anaheim, CA, USA, 2019, pp. 1629-1634.

[2] A. A. Huzayyin, "Utilizing the nonlinearity of a magnetic core inductor as a source of variable reactive power compensation in electric power systems," in Proc. Annu. IEEE Conf. Student Paper, 2008, pp. 1–4.

[3] S. Aldhaher, P. C.-K. Luk, and J. F. Whidborne, "Electronic tuning of misaligned coils in wireless power transfer systems," IEEE Trans. Power Electron., vol. 29, no. 11, pp. 5975–5982, Nov. 2014.

[4] L. Zhang, W. G. Hurley, and W. H. Wölfle, "A new approach to achieve maximum power point tracking for PV system with a variable inductor," IEEE Trans. Power Electron., vol. 26, no. 4, pp.1031–1037, Apr. 2011.

[5] M. S. Perdigao, J. M. Alonso, M. A. Dalla Costa, and E. S. Saraiva, "Using magnetic regulators for the optimization of universal ballasts," IEEETrans.PowerElectron.,vol.23,no.6,pp.3126–3134,Nov.2008.

[6] E. Orietti, P. Mattavelli, G. Spiazzi, C. Adragna, and G. Gattavari, "Two-phase interleaved LLC resonant converter with current controlled inductor," in Proc. Brazilian Power Electron. Conf., 2009, pp. 298–304.

[7] M. S. Perdigão, M. F. Menke, Á. R. Seidel, R. A. Pinto and J. M. Alonso, "A Review on Variable Inductors and Variable Transformers: Applications to Lighting Drivers," in IEEE Transactions on Industry Applications, vol. 52, no. 1, pp. 531-547, Jan.-Feb. 2016.

[8] H. Fan and H. Li, "High-Frequency Transformer Isolated Bidirectional DC–DC Converter Modules with High Efficiency Over Wide Load Range for 20 kVA Solid-State Transformer," in IEEE Transactions on Power Electronics, vol. 26, no. 12, pp. 3599-3608, Dec. 2011.

[9] Burgio, A.; Menniti, D.; Motta, M.; Pinnarelli, A.; Sorrentino, N.; Vizza, P., "A laboratory model of a dual active bridge DC-DC converter for a smart user network," in Environment and Electrical Engineering (EEEIC), 2015 IEEE 15th International Conference on, vol., no., pp.997-1002, 10-13 June 2015.

[10] Ferreira, Samuel Filipe Soares. Electromagnetic study of a variable inductor controlled by a DC current. MS thesis. University of Coimbra, 2016.

[11] S. Saeed, J. Garcia, M. S. Perdigão, V. S. Costa, B. Baptista and A. M. S. Mendes, "Improved inductance calculation in variable power inductors by adjustment of the reluctance model through magnetic path analysis," 2019 IEEE Energy Conversion Congress and Exposition (ECCE), Baltimore, MD, USA, 2019, pp. 6634-6640.

[12] Orenchak, George. "Predicting Temperature Rise of Ferrite Cored Transformers." (2017).

[13] D. Medini and S. Ben-Yaakov, "A current-controlled variable inductor for high frequency resonant power circuits," in Proc. IEEE APEC, 1994, pp. 219–225.

[14] J. M. Alonso, G. Martínez, M. Perdigão, M. Cosetin and R. N. do Prado, "Modeling magnetic devices using SPICE: Application to variable inductors," 2016 IEEE Applied Power Electronics Conference and Exposition (APEC), Long Beach, CA, 2016, pp. 1115-1122.

[15] S. Saeed, J. García and R. Georgious, "Modeling of variable magnetic elements including hysteresis and Eddy current losses," 2018 IEEE Applied Power Electronics Conference and Exposition (APEC), San Antonio, TX, 2018, pp. 1750-1755.

[16] Ferreira, Samuel Filipe Soares. Electromagnetic study of a variable inductor controlled by a DC current. MS thesis. University of Coimbra, 2016.

[17] E. A. Bitencourt, M. R. Cosetin, I. G. Vegner and R. N. do Prado, "A ferromagnetic based variable inductor analysis and design methodology," 2015 IEEE 13th Brazilian Power Electronics Conference and 1st Southern Power Electronics Conference (COBEP/SPEC), Fortaleza, 2015, pp. 1-5.

[18] Van den Bossche, Alex, and Vencislav Valchev. "Thermal design of transformers and inductors in power electronics." 4ième Conférence internationale sur le Génie Electrique (CIGE 2010). No. 2. Université de Bechar Algérie, 2010.

[19] Pico Technology Ltd., PicoLog: https://www.picotech.com/data-logger/tc-08/thermocouple-data-logger

[20] George G. Orenchak, Estimating Temperature rise of transformers [Online]. Available: http://www.tscinternational.com/tech12.pdf

[21] S. S. Ben-Yaakov, "SPICE simulation of ferrite core losses and hot spot temperature estimation," 2017 24th IEEE International Conference on Electronics, Circuits and Systems (ICECS), Batumi, 2017, pp. 107-110, doi: 10.1109/ICECS.2017.8292005.

[22] Altair Flux™ [Online]. Available: https://altairhyperworks.com/product/flux#